DR ANNE-PAULINE BELLANGER (Orcid ID : 0000-0003-4144-476X)
PROFESSOR BRITTA LUNDSTRÖM-STADELMANN (Orcid ID : 0000-0003-2672-5766)
DR JUNHUA WANG (Orcid ID : 0000-0002-6110-3711)

Article type : Original Paper

Innate and adaptive immune responses following PD-L1 blockade in treating chronic murine alveolar echinococcosis

Short title: PD-L1 blockade in treating chronic murine AE

Fadi Jebbawi[1], Anne-Pauline Bellanger[2,3], Britta Lunström-Stadelmann[4], Reto Rufener[4], Michel Dosch[1], Christine Goepfert[5], Bruno Gottstein[6], Laurence Millon[2,3], Denis Grandgirard[6], Stephen L. Leib[6], Guido Beldi[1*], Junhua Wang[4,6*]

1. Department of Visceral Surgery and Medicine, Inselspital, University Hospital of Bern, Bern, Switzerland
2. Chrono-Environment UMR/CNRS 6249, University of Bourgogne Franche-Comté, Besançon, France
3. Parasitology Mycology Department, University Hospital Jean Minjoz, Besancon, France

This article has been accepted for publication and undergone full peer review but has not been through the copyediting, typesetting, pagination and proofreading process, which may lead to differences between this version and the Version of Record. Please cite this article as doi: 10.1111/PIM.12834

4. Institute of Parasitology, Department of Infectious Diseases and Pathobiology, Vetsuisse Faculty, University of Bern, Bern, Switzerland
5. Institute of Animal Pathology, COMPATH, Department of Infectious Diseases and Pathobiology, Vetsuisse Faculty, University of Bern, Switzerland.
6. Institute for Infectious Diseases, University of Bern, Bern, Switzerland
Correspondence to: Dr. Junhua Wang, PhD, Institute for infectious diseases, University of Bern, Friedbühlstrasse 51, 3010 Bern, Switzerland. E-mail: junhua.wang@ifik.unibe.ch. Tel.: +41 31 631 25 93
*These two authors equally contributed as senior authors
Disclosures: None.

Data availability statement

Data openly available in a public repository that issues datasets with DOIs: The data that support the findings of this study are openly available in [pubmed] at http://doi.org/[doi].

Author contributions

JW designed the study. JW, FJ, APB, RR, MD, CG conducted the experimental work and analyzed the data. JW performed parasitic infection in mice and collected samples. BG, BS, GB, LM, SL, DG and JW designed and supervised the experiments in the presented study. FJ and JW wrote the original draft. BG, GB, LM, SL and DG contributed to the revised manuscript.

Abstract

Background: Programmed death-1 (PD-1) and programmed death ligand-1 (PD-L1) immune checkpoint blockade is efficacious in certain cancer therapies.

Objectives: The present study aimed to provide a picture about the development of innate and adaptive immune responses upon PD-L1 blockade in treating chronic murine AE.

Methods: Immune treatment started at 6 weeks post *E. multilocularis*-infection, and was maintained for 8 weeks with twice per week anti-PD-L1 administration (intraperitoneal). The study included an outgroup-control with mice perorally medicated with albendazole five days/week, and another one with both treatments combined. Assessment of treatment efficacy was based on determining parasite weight, innate and adaptive immune cell profiles, histopathology, and liver tissue cytokine levels. **Results/conclusions:** Findings showed that the parasite load was significantly reduced in response to PD-L1 blockade, and this blockade a) contributed to T cell activity by increasing $CD4^+$/$CD8^+$ effector T cells, and decreasing Tregs; b) had the capacity to re-store DCs and Kupffer cells/Macrophages; c) suppressed NKT and NK cells; and thus d) lead to an improved control of *E. multilocularis* infection in mice. This study suggests that the PD-L1 pathway plays an important role by regulating adaptive and innate immune cells against *E. multilocularis* infection, with significant modulation of tissue inflammation.

Key words: *Echinococcus multilocularis*; anti-PD-L1; immunotherapy; albendazole

Introduction

Alveolar echinococcosis (AE) is one of the clinically most severe zoonotic helminthic diseases in humans, caused by the continuous proliferation of the larval stage (metacestode) of *Echinococcus multilocularis*. Upon ingestion of the *E. multilocularis* eggs by intermediate hosts such as small rodents and human, echinococcal metacestodes form alveolar structures with multiple vesicles of different sizes within the liver. In humans, the severity of this disease results from both a continuous asexual proliferation of the metacestode and an intense inflammatory granulomatous infiltration around the parasite which causes pathological damages in the liver. The lesions act like a slow-growing liver cancer, progressively invading the neighboring tissues and organs (1). During the past decades, the AE case incidence has significantly increased in Switzerland. This is due to a high environmental contamination with parasite eggs through very high fox population density, and also opportunistically due to an increased number of patients receiving immunosuppressive therapy that renders them more susceptible to AE infection and disease (2,3). Mechanistically, AE patients present a periparasitically down-regulated immune response that is triggered by the parasite such as to orient immunity towards anergy. Different treatment options of AE primarily depend on the metacestode tissue size and location: first choice is a radical (curative) resection of the parasite by surgery (3,4). If not feasible, long-term to life-long daily medication with albendazole (ABZ) provides a good health improvement in many of the patients, but this approach is frequently not curative (5). Thus, new alternative curative treatment strategies are needed, and a respective focus on the appropriate support of the immune system for a better control of the infection appears highly attractive (6–8).

Previous studies showed that an initial acute inflammatory Th1 response (putatively immune protective) is gradually converting into a mixed Th1/Th2 response during the chronic phase of AE, allowing parasite survival upon regulation via $CD4^+CD25^+Foxp3^+$ T (Treg) cells and Th17 cells, and thus finally leading to a lethal outcome of disease due to continuous long-term parasite proliferation and maturation (6). The presence and expression level of the programmed cell

death-1 (PD-1) and PD-L1 has a major role in the inhibition of effector T-cell function (9). Antibodies targeting those immune check points are in clinical use (pembrolizumab and nivolumab) and are showing promising results to treat various forms of cancer (10), and infectious diseases (7). With regard to echinococcosis, significantly higher levels of sPD-L1 in patients with cystic echinococcosis were observed compared with healthy controls, and elevated levels of Th2 cytokines in the sera of patients with CE (11). In one of our previous studies in mice (12), anti-PD-L1 administration significantly decreased parasite growth when compared to non-treated animals, and the effect was associated with an increased Th1 response in the secondary AE model (intraperitoneal infection with metacestodes), and decreased Treg/Th2 responses in the natural primary AE model (oral infection with eggs). This preliminary study aimed to test whether PD-L1 blockade protects against both primary and secondary infection mouse models. We blocked PD-L1 before *E. multilocularis* infection, and mainly focused on the effect of PD-L1 blockade by using two models in murine AE. These models revealed that, the immune response mediated by T cells and Tregs upon PD-L1 blockade was protective against murine AE.

However, to date, few immunological studies have been undertaken to characterize the adaptive and innate immune response in detail as a result of PD1/PD-L1 blockade during *E. multilocularis* infection. The same lack refers also to conventional ABZ treatment as a standard control. In order to address the potential clinical implications of PD-L1 blockade for patients who do not respond to albendazole treatment, we mimicked a chronic AE infection by using a secondary infection model. Here we blocked the PD-L1 pathway at the chronic stage of *E. multilocularis* infection as a treatment, and the conventional chemotherapy with albendazole or a combined therapy as controls. The aims of this study were thus: 1) to investigate the immune checkpoint blockade in *E. multilocularis* infected mice, using the PD-1/PD-L1 axis and immune parameter assessment in the liver and exudate peritoneal cells (PECs); 2) to give a comprehensive picture on the immune system dynamics during *E. multilocularis* infection, in response to PD-L1 blockade and as an outgroup control, to conventional ABZ treatment. To address these questions,

we applied a long period (2 months) of treatment (using two different approaches: immunotherapy and/or medication with ABZ) in the intraperitoneal-infection mouse model (secondary infection model), mimicking a chronic and rather advanced, but not final stage of infection for human patients.

Materials and Methods

Ethics Statement

The animal studies were performed in accordance with the recommendations of the Swiss Guidelines for the Care and Use of Laboratory Animals. The protocol was approved by the governmental Commission for Animal Experimentation of the Canton of Bern (approval no. BE112/17).

Experimental design, infection, and treatments

Mice. 48 Female 8-week-old wild type C57BL/6-mice were purchased from Charles River GmbH (Sulzfeld, Germany), and divided randomly into 8 groups (6 mice each group) as follows: 1) *E. multilocularis* infected (named as "AE"); 2) non-infected control (named as "Control"); 3) *E. multilocularis* infected + αPD-L1 blocking (named as "AE-αPD-L1"); 4) non-infected + αPD-L1 blocking (named as "Control-αPD-L1"); 5) *E. multilocularis* infected + αPD-L1 blocking + ABZ (named as "AE-αPD-L1+ABZ"); 6) non-infected + αPD-L1 blocking + ABZ (named as "Control-αPD-L1+ABZ"); 7) *E. multilocularis* infected + ABZ (named as "AE-ABZ"); 8) non-infected + ABZ (named as "Control-ABZ"). All animals were housed in a standard daylight/night cycle room with food and water according to recommendations of the Federation of European Laboratory Animal Science Association (FELASA), and they were monitored by daily inspection, including the assessment of the appearance of health status, putative weight loss or gain during the whole course of the experiment. All experiments with animals were performed within a laminar flow safety enclosure.

Parasite preparation and intraperitoneal infection of mice. Intraperitoneal infection with *E.*

multilocularis metacestodes was performed as previously described (13). Briefly, *E. multilocularis* (H95) was isolated and maintained by serial passages (vegetative transfer) in C57BL/6 mice. In order to prepare the infection material for mice, metacestode tissue was obtained from previously infected mice by aseptic removal from the peritoneal cavity. After grinding the tissue through a sterile 50 µm sieve, approximately 100 freshly prepared vesicular cysts were suspended in 100 µL sterile PBS (Gibco, Basel, Switzerland) and intraperitoneally injected. Each experimental group included 6 animals unless otherwise stated. Control mice received 100 µL of sterile PBS only.

Treatments. Groups 1&2 received 100 µL PBS by i.p. injection twice/week and 100 µL corn oil perorally 5 times/week. Groups 3&4 received 100 µL αPD-L1 MAb (200 µg/mouse/injection, BioXcell, clone 10F.9G2, West Lebanon, USA) by i.p. injection twice/week and 100 µL corn oil perorally 5 times/week. Groups 5&6 received 100 µL αPD-L1 MAb (200 µg/mouse/injection) by i.p. injection twice/week, and 100 µL ABZ in corn oil (200 mg/kg mouse /injection, Sigma, Buchs, Switzerland) perorally 5 times/week. Groups 7&8 received 100 µL ABZ in corn oil (200 mg/kg mouse/injection) perorally 5 times/week and 100 µL PBS by i.p. injection twice/week. All the treatments start at 6 weeks post infection and maintain for another 8 weeks.

Sampling. At the end of experiments, mice were sacrificed by CO_2-euthanasia. *E. multilocularis* metacestode vesicles are filled with vesicle fluid (VF), intact parasite tissues were surgically recovered and, if present, fat and connective tissues were carefully removed for subsequent wet-weight determination of the parasite mass (12).

Liver cells were isolated by using percoll density gradient centrifugation (see below), and peritoneal exudate cells (PECs) were collected by peritoneal rinsing.

Histopathology and histopathological grading. Liver sections and parts of the parasites from *E. multilocularis*-infected mice were fixed in 10 % neutral buffered formalin for 24 hours and embedded in paraffin. Blocks were sectioned and slides were stained with hematoxylin and eosin (H&E). The macroscopic and microscopic evaluations were performed in a blinded fashion by a European board-certified veterinary pathologist.

Cell preparation

Livers were perfused with PBS via the portal vein until blanched and then put in IMDM, supplemented with 10% fetal bovine serum (FBS). Whole livers were passed through a metal filter and digested with 0.05% collagenase IV (Worthington Biochemical, Allschwil, Switzerland) and 0.001% DNAse I (Sigma-Aldrich, Buchs, Switzerland) for 30 min at 37 °C as described by Huang Li (13). Intrahepatic mononuclear cells were purified on a percoll gradient after centrifugation at 1,250 g for 20 min without braking. Peritoneal exudate cells (PEC) were collected by peritoneal rinsing with 5 mL RPMI-1640. Cells were subsequently washed twice with, and then re-suspended in PBS containing 3% FBS for cell staining.

Flow cytometry

Aliquots of 10^6 cells/100 µL of staining buffer per well were incubated each with 1 µg of purified anti-CD16/CD32 for 20 min in the dark, in order to block non-specific binding of antibodies to the FcγIII and FcγII receptors. Cell suspensions were incubated with a cell viability dye efluor 506 20 nm 4 °C in the dark (Thermo Fisher Scientific) to exclude dead cells. Subsequently, these cells were separately stained with the following surface markers for 20 min with 1 µg of primary antibodies (Table 1). For cytokines and transcription factors, cells subsequently fixed and permeabilized according to the manufacturer's instructions (Foxp3/Transcription Factor Staining Buffer Set; eBioscience). Corresponding fluorochrome-labeled isotype control antibodies were used for staining controls. Cells resuspended in 250 µL of buffer (0.15 M NaCl, 1 mM NaH_2PO_4 H_2O, 10 mM Na_2HPO_4 $2H_2O$ and 3 mM NaN_3) were analyzed in a flow cytometer BD LSR II (BD Pharmingen Inc., San Diego, CA) using the corresponding BD FACSDiva software (S1 Fig). Flow cytometric analysis was done using FlowJo software (Treestar, Inc., Ashland, OR). The gating strategy was shown in S1 Fig.

Cytokine levels from liver cell lysates measured by Mesoscale

Cells were lysed using RIPA buffer (Sigma–Aldrich), containing protease inhibitor cocktail (Roche, Basel, Switzerland), and centrifuged at 14,000 × *g* for 20 min at 4 °C. Proteins were

quantified using Bradford assay kit from Abcam and 40 ug of proteins were used for mesoscale. Each biotinylated antibody was conjugated to the assigned linker with incubating at room temperature for 30 min. After 30 min in stop solution, all the U-PLEX-coupled antibody solution was pooled and mixed by vortexing. The U-PLEX plate was coated by adding 50 µL of multiplex coating solution to each well at 4 °C overnight and then washed 3 times with 150 µL/well of 1× PBS-T (PBS with 0.05% Tween-20). After adding 25 µL dilute 41 to each well, 25 µL of prepared Calibrator standard or samples (non-diluted serum or 40 µg liver cell lysates) was added and incubated at room temperature with shaking for 1 hour. After 3 washes with 150 µL/well of 1× PBS-T, 50 µL of detection antibody solution was added to each well and incubated at room temperature with shaking for 1 hour. After 3 washes with 150 µL/well of 1× PBS-T. 150 µL/well of 2× Read Buffer T was added. The plated was analyzed on MESO QuickPlex SQ 120 (Rockville, Maryland, USA).

Statistical analyses

All data were analyzed by Prism Graphpad. The results are presented as means ± SD. Normality of data was assessed by D'Agostino & Pearson and Shapiro-Wilk test. For normally distributed groups of data, One-way ANOVA with Bonferroni's correction was used to compare the differences between groups. Levels of significance were assessed with specifically indicated tests and p-values are presented as follows: *p<0.05; **p<0.01;***p<0.001;****p<0.0001.

Results

Significantly decreased parasite load in AE mice with PD-L1 blockade or ABZ treatment

In mice intraperitoneally infected with *E. multilocularis* metacestodes, the parasite load was significantly reduced in response to PD-L1 blockade (AE- αPD-L1; 2.46 ± 1.59 g) when compared to mock-treated AE mice (AE; 5.47 ± 3.37 g) (Fig 1A, *P*=0.0068). In ABZ treated AE mice (AE-ABZ), parasite weight was 0.36 ± 0.18 g, while it was 0.22 ± 0.08 g in AE mice with a

combined treatment of αPD-L1 with ABZ (AE- αPD-L1+ABZ); they were significantly lower when compared to mock-treated AE mice (Fig 1A, P=0.0001). The combination of PD-L1 blockade and ABZ treatment did not lead to a statistically significant differences in parasite weight when compared to AE-ABZ (Fig 1A, $P>0.05$), thus we further focused on the mechanism of PD-1/PD-L1 ligation and ABZ individually in the immunological defense against AE.

Significant decrease of inflammation in AE mice with αPD-L1 administration

Upon macroscopical and histological assessment, none of the livers from any animal included any visible parasitic structures. Mixed inflammatory cell infiltrates (mostly including lymphocytes, eosinophils, and neutrophils) were, however, detectable in livers of animals from all groups (S2 Fig). Extramedullary hematopoiesis (EMH) became apparent in AE mice with significant decrease in $CD45^+$ hepatic immune cells compared to non-infected control animals, representing a higher need of immune cells in the fight against infection (S3 Fig; <0.0001). Moreover, expression of the inflammatory cytokines TNF-α (Figure 1B; P=0.0004), IL-1β (Fig 1C; P=0.0002), IL-6 (Fig 1D; P=0.0004), IFN-γ (Fig 1E; P=0.0002) and IL-33 (Fig 1F; P=0.0006) was significantly higher in AE mice when compared to non-infected control animals (Fig 1B-F). In the livers from AE mice treated with αPD-L1, there was a decrease in the inflammatory cytokines TNF-α (Figure 1B; P=0.0005), IL-1β (Fig 1C; P=0.0002), IL-6 (Fig 1D; P<0.0001) and IL-33 (Fig 1F; P<0.0001), and an increase in $CD45^+$ hepatic immune cells (S3 Fig; P<0.0001), when compared to mock-treated AE mice. However, there was no difference in IFN-γ levels between AE- αPD-L1 and mock-treated AE mice (Fig 1E).

Increased $CD4^+$ / $CD8^+$ Teffs and decreased Tregs from AE mice with αPD-L1 administration

Flow cytometric analyses showed that there was a significant increase of $CD4^+$ Teff cells (Fig 2A; P<0.0001) and $CD8^+$ Tcyt cells (Fig 2C & S4 Fig; P<0.0001) in the livers from AE-αPD-L1 mice, when compared to mock-treated AE mice. Moreover, AE-αPD-L1 mice also showed a decreased

CTLA$^+$ frequency in both CD4$^+$ Teffs and CD8$^+$ Tcyts, when compared to mock-treated AE mice (Fig 2B; P=0.0051, 2D; P<0.0001). ABZ treatment improved CD8$^+$ Tcyts but not CD4$^+$ Teffs (Fig 2A; P=0.4908, 2C; P=0.0414; S4 Fig) when compared to mock-treated AE mice.

In the livers and peritoneal exudate cells (PECs) from AE mice, a significant increase of regulatory T cells (CD4$^+$ (Fig 2E; P<0.0001, 3E; P<0.0001) and CD8$^+$ Tregs (Fig 2G; P<0.0001, 3G P<0.0001) became apparent, when compared to non-infected controls. Both CD4$^+$ and CD8$^+$ Treg frequency decreased significantly in the livers and PECs from AE-αPD-L1 mice when compared to mock-treated AE mice (Fig 2E, 3E). Moreover, there was a decrease of both CD4$^+$ and CD8$^+$ Treg cells in the livers and PECs from AE-ABZ mice when compared to mock-treated AE mice (Fig 2E, 3E). Moreover, IL-10 expression levels secreted by CD45$^+$ cells increased significantly in AE mice when compared to non-infected controls (S5 Fig; P=0.0054), decreased in AE-αPD-L1 mice (S5 Fig; P=0.0038) but not in AE-ABZ mice when compared to AE mice (S5 Fig; P=0.09). To sum up, PD-L1 blockade led to an increased CD4$^+$ and CD8$^+$ T cell activity in AE mice, while ABZ showed a partial improvement for CD8$^+$ T cells.

Dendritic cells, Kupffer cells/Macrophages were restored in AE mice with αPD-L1 administration

The role of innate immune cells such as dendritic cells (Plasmacytoid DCs, pDCs: CD11c$^+$ CD11b$^-$DCs; Classical DCs, cDCs: CD11b$^+$CD11c$^+$ DCs) and Kupffer cells (CD11c$^+$CD11b^{dim} F4/80$^+$) was studied to assess their ability to express PD-L1. A 10-fold decrease in CD11c$^+$ pDCs (Fig 4A; P<0.0001; S6 Fig), and a 2-fold decrease in CD11c$^+$ Kupffer cells (Fig 4C; P<0.0001; S6 Fig) was observed in the livers from AE mice when compared to non-infected control animals. Interestingly, there was an increase of pDCs in the livers (Fig 4A; P<0.0001; S6 Fig), CD11c$^+$ CD11b$^+$ DCs in PECs (Fig 4E; P<0.0001; S6 Fig), and CD11c$^+$ Kupffer cells in the livers and CD11c$^+$ Macrophages in PECs (Fig 4C, F; P<0.05; S6 Fig) from AE-αPD-L1 mice when compared to mock-treated AE mice. However, ABZ did not show any effect on innate immune cells in AE mice (Fig 4A-F).

NKT and NK cells decreased in the liver from AE mice upon αPD-L1 administration

A significant increase of NKT and NK cell frequency was observed in the livers from AE mice when compared to non-infected control animals (Fig 5A, C; $P<0.0001$; S6 Fig). Moreover, both NKT and NK cell frequency and activation ($CD69^+$) were significantly decreased in the livers from AE-αPD-L1 mice, when compared to AE mice (Fig 5B, D; $P<0.0001$; S6 Fig). However, a significant decrease of hepatic NK cells but not NKT was observed in AE-ABZ mice when compared to the AE group (Fig 5A, C; $P<0.0001$) without significant decrease of CD69 frequency as in AE-αPD-L1 group when compared to mock-treated AE mice (Fig 5B, D).

Discussion

In the present study, we investigated adaptive and innate immune cell dynamics at the chronic stage of *E. multilocularis* infection and the effect of anti-PD-L1 and/or ABZ administration on the parasite growth via immune system. We showed for the first time PD-L1 immune checkpoint blockade as a new treatment against chronic AE in mice, and demonstrated that the PD-L1 pathway a) contributes to T cell activity by increasing $CD4^+$/$CD8^+$ effector T cells and decreasing Tregs; b) has the capacity to re-store DCs and Kupffer cells/Macrophages; c) suppresses NKT and NK cells; and d) leads to an improved control of *E. multilocularis* infection in mice (Fig 6).

E. multilocularis infection is characterized by modulation of the immune response of the host (14–16), during AE, a down-regulation of protective immunity in parallel with a Th2-reorientation of the $CD4^+$ T lymphocytes and respective induction of an immunotolerant or anergic response to infection (3,17–19). Recent studies have shown that T cell exhaustion took part in the overall metacestode growth at late stage of infection in mice (20). Prevention of T-cell exhaustion e.g. by *in vivo*-blocking TIGIT (liver T-cell immunoreceptor with immunoglobulin and immunoreceptor tyrosine-based inhibitory motif domain) could inhibit disease progression in *E. multilocularis*-infected mice (18). Mechanistically, $CD4^+$ T cells were totally and $CD8^+$ T cells partially required for anti-TIGIT-induced regression of parasite growth in mice (21). Several

studies established the importance of PD-1/PD-L1 immune checkpoint blockade on T cells proliferation capacity and function in context of *Taenia*, *Schistosoma* and *Leishmania amazonensis* infections(22–24). In another study, Smith *et al*. and Terrazas *et al*. showed that blocking PD-L1 (*Shistozoma,Taenia*) and or PD-L2 (*Taenia*) blocked the ability macrophages to anergize T cells in *Schistozoma* and *Taenia* infected mice (25). Joshi *et al*. demonstrated the importance of PD-1/PD-L1 ratio in suppressing $CD8^+$ Tcells during *L. donovani* infection. Using anti-PD-1 antibodies, they could increase the proliferative capacity of $CD4^+$ and $CD8^+$ T cell populations, and recovery of IFN-γ production (26). The PD-1/PD-L1 pathway negatively regulates T cells during priming and also the effector phase, when T cells act on the target cells; it thus appears as a major regulator of T-cell exhaustion (27). In the present study we showed that blocking the PD-L1 pathway restored both $CD4^+$ and $CD8^+$ T cells and improved the control of *E. multilocularis* infection. It indicated that improving $CD4^+$ and/or $CD8^+$ effector T cell function could still be the main option in treating AE. As shown by several studies (14-16), there exist a mixed response with Th1 and Th2 biasing at different kinetic windows. And a Th2 dominant response at chronic AE, preferentially might also induce PD-L2 (possibly via STAT6), as opposed to PD-L1, the latter of which has been neutralized in this study. PD-L2 could be a potential target as well in treating AE, and needs to be further studied.

Distinctive characteristics of PD-1 expression on peripheral Tregs in HCV infection suggests associated with impaired adaptive immunity as well as viral long-term persistence (37). In the present and other studies, Treg cells significantly increased in both AE mice (8,11,12,38) and AE patients during the progressive course of disease (39). In this current study, this is reflected by an immuno-feedback regulation of T cell expansion in the liver, leading to an immune imbalance in favor for the parasite survival and development. In one of our previous studies, where we used a DEREG mouse model, we showed that *E. multilocularis* growth in AE mice with $Foxp3^+$ Tregs-depletion yielded significantly smaller average AE lesions in the liver when compared to those without $Foxp3^+$ Tregs-depletion. This phenomenon was associated with a higher Th1 immune response, a lower IL-10 production, no difference of Th2/Th17 immunity, and

up-regulation of APC activation (38). Based on these findings on the role of Foxp3$^+$ Tregs in *E. multilocularis* infection, we showed in this current study that the treatment of *E. multilocularis*-infected mice with Foxp3$^+$ Tregs-blocking agents (i.e. PD1/ PD-L1 blockade) could provide a means of converting the immunological anergy during chronic disease into a more pro-active, improved CD4$^+$/CD8$^+$ effector T cell function and a decreased Treg activity. Moreover, this could also induce a Th1-oriented immune polarization (11), with potentially damaging or even fatal consequences for the metacestode, and thus a putatively healing option for the host.

DCs play a major role as antigen presenting cells with high capacity of stimulating T cells in the *in vitro* mixed leucocyte reaction (43), and they secrete IL-2, which stimulate T cells by expanding those specific for *E. multilocularis* (17,18,44,45). In this study, we found that at the chronic infection stage, cDCs in the liver were significantly decreased, accompanied by an increase of CD4$^+$ and CD8$^+$ Treg cells and a decrease in CD4$^+$ Teff and CD8$^+$ Tcyt. Moreover, PD-L1 blockade in AE mice restored and inversed significantly the Treg/Teff ratio. This had already been previously demonstrated that blocking PD-L1 on DCs against melanoma increased Th1 and Th17 proliferation, concomitant with a Treg reduction, independently of the DCs' phenotype and functional characteristics (19).

Shi *et al.* showed that Kupffer cells are susceptible to apoptosis after infection with microorganisms at the terminal stage of Trypanosoma infection in the presence of IFN-γ (50,51). Based on the fact that Kupffer cells express PD-L1, we hypothesized that they might also be involved in the PD-1/PD-L1 immune axis checkpoint. Interestingly, we observed a significant decrease in CD11c$^+$ Kupffer cells in AE mice when compared to non-infected controls. Moreover, PD-L1 blockade restored CD11c$^+$ Kupffer cells and CD11c$^+$ macrophages in PECs. The increase of macrophage recruitment to the site of infection suggests that Kupffer cells, suppressed by Treg cells during the infection, are playing a major role in parasite clearance (52). However, in the current study, Kupffer cells were not associated with an increase of inflammation with PD-L1

blockade. Their role remains still unclear, further mechanistic studies will have to be included in our ongoing and future projects.

NK and NKT cells are also major players in maintaining immune homeostasis, and first responders for infections (56–58). NK cells in the liver are very frequent, divided between cNK ($CD49b^+$ NK) and resident NK cells ($CD49a^+$ NK) (59–62). In this present study, total NK cells were significantly increased due to *E. multilocularis* infection, with also an increasing of NKT cells. NK cells are reported to be protective at the early stages of parasitic infections. It is known that Listeria induces the production of both TNF-α and IL-12 by macrophages, which subsequently activate NK cells (63–65). This might explain how inflammatory cytokines induce NK cells in *E. multilocularis* infected mice (AE group). And this was supported by the data from suppl Fig.7, which in AE group there was a conversion from ILC-1 to NK cells. This conversion was reversed in AE mice with PD-L1 blockade. We hypothesized that these populations of NK cells with decreased inflammatory cytokines might be "exhausted NK cells", but this needs to be further confirmed by functional assays. This is already under study.

ABZ, as a positive control, is very efficient against *E. multilocularis* infection in mice. Long-term to life-long daily medication with ABZ provides a good health improvement in many of the patients, but it is only periparasitic and this approach is thus frequently not curative. Moreover, some patients do not respond to ABZ treatment and suffer from very aggressive lesions under ABZ therapy. Studies have shown that patients with cystic echinochoccosis (CE) and low CD4 counts have poor response to ABZ treatment, and continuous ABZ therapy was ineffective in HIV-infected patients with CE and low CD4 counts (70). Nowadays, possibly because of the more frequent use of immuno-suppressive drugs in the clinics, more and more patients become ABZ resistant. New alternative curative treatment strategies are urgently needed, and a respective focus on the appropriate support of the immune system i.e. our study documented the immune cell dynamic/interaction network at the chronic stage of *E. multilocularis* infection, with PD-L1 blockade as a new treatment option. PD-L1 blockade is promising against larval stage of *E. multilocularis* infection by improving protective immunity, with less global liver inflammation.

Such an approach could be coupled with a short term anti-PD-L1 administration to improve a protective immune orientation in AE patients, and, putatively coupled to ABZ medication, it could optimize the inhibition of the parasite growth, or maybe even abrogate parasite viability, thus putatively leading to cure.

Acknowledgements

Fadi Jebbawi was supported by the International Fellowship Program on Integrative Kidney Physiology and Pathophysiology (IKPP). This work was supported by the Swiss National Science Foundation 160108 to BG 179439 to BLS and 189136 to SLL) and the National Reference Center for Echinococcosis coordinated by Prof. L. Millon (University Hospital J Minjoz, Besancon, France). This project has received funding within the frame of IKPP2 from the European Union's Seventh Framework Programme for research, technological development and demonstration under the grant agreement no 608847.

References

1. Vuitton DA, Zhang SL, Yang Y, Godot V, Beurton I, Mantion G, et al. Survival strategy of *Echinococcus multilocularis* in the human host. Parasitol Int. 2006; 55:S51–5.
2. Schweiger A, Ammann RW, Candinas D, Clavien PA, Eckert J, Gottstein B, et al. Human alveolar echinococcosis after fox population increase, Switzerland. Emerg Infect Dis. 2007;13(6):878–82.
3. Salm LA, Lachenmayer A, Perrodin SF, Candinas D, Beldi G. Surgical treatment strategies for hepatic alveolar echinococcosis. Food Waterborne Parasitol. 2019; 1:15.
4. Sarwari AR. Advances in Parasitology—Echinococcus and Echinococcosis, Part A. Clin Infect Dis. 2018; 66(10):1649–1649.
5. De Rosa F, Teggi A. Treatment of *Echinococcus granulosus* hydatid disease with albendazole. Ann Trop Med Parasitol. 1990; 84(5):467–72.

6. Wang J, Cardoso R, Marreros N. Foxp3$^+$ T Regulatory Cells as a Potential Target for Immunotherapy against Primary Infection with *Echinococcus multilocularis* Eggs. Infect Immun. 2018; 86(10): e00542–18.
7. Bhadra R, Gigley JP, Weiss LM, Khan IA. Control of Toxoplasma reactivation by rescue of dysfunctional CD8$^+$ T-cell response via PD-1-PDL-1 blockade. Proc Natl Acad Sci. 2011; 108(22):9196–201.
8. La X, Zhang F, Li Y, Li J, Guo Y, Zhao H, et al. Upregulation of PD-1 on CD4$^+$CD25$^+$T cells is associated with immunosuppression in liver of mice infected with *Echinococcus multilocularis*. Int Immunopharmacol. 2015; 26(2):357–66.
9. Pardoll DM. The blockade of immune checkpoints in cancer immunotherapy. Nat Rev Cancer. 2012; 12(4):252–64.
10. De Lichtenberg TH, Hermann GG, Rørth M, Højer Larsen M-J, Mansourvar Z, Holm ML, et al. Overall survival after immunotherapy, tyrosine kinase inhibitors and surgery in treatment of metastatic renal cell cancer: outcome of 143 consecutive patients from a single centre. Scand J Urol. 2014; 48(4):379–86.
11. Li *et al.,* Role of soluble programmed death-1 (sPD-1) and sPD-ligand 1 in patients with cystic echinococcosis. Exp Ther Med. 2016; **11**: 251-256.
12. Wang J, Jebbawi F, Bellanger A-P, Beldi G, Millon L, Gottstein B. Immunotherapy of alveolar echinococcosis via PD-1/PD-L1 immune checkpoint blockade in mice. Parasite Immunol. 2018; 40(12):e12596.
13. Wang J, Vuitton DA, Müller N, Hemphill A, Spiliotis M, Blagosklonov O, et al. Deletion of Fibrinogen-like Protein 2 (FGL-2), a Novel CD4$^+$ CD25$^+$ Treg Effector Molecule, Leads to Improved Control of *Echinococcus multilocularis* Infection in Mice. PLoS Negl Trop Dis. 2015; 9(5):e0003755.
14. Wang J, Gottstein B. Immunoregulation in larval *Echinococcus multilocularis* infection. Parasite Immunol. 2016; 38(3):182–92.
15. Gottstein B, Hemphill A. *Echinococcus multilocularis*: The parasite–host interplay. Exp

Parasitol. 2008; 119(4):447–52.

16. Vuitton DA, Zhang SL, Yang Y, Godot V, Beurton I, Mantion G, et al. Survival strategy of *Echinococcus multilocularis* in the human host. Parasitol Int. 2006; 55:S51–5.
17. Wuest SC, Edwan J, Martin JF, Han S, Perry JSA, Cartagena CM, et al. A vital role for IL-2 trans-presentation in DC-mediated T cell activation in humans as revealed by daclizumab therapy. Nat Med. 2011; 17(5):604.
18. Feau S, Facchinetti V, Granucci F, Citterio S, Jarrossay D, Seresini S, et al. Dendritic cell-derived IL-2 production is regulated by IL-15 in humans and in mice. Blood. 2005;105(2):697–702.
19. Lopez M, Behrens C, Falcon-Beas C, Tempio F, Salazar-Onfray F. Blocking of PD-L1 on therapeutic dendritic cells modulate in vitro T cells proliferation and differentiation to Th1 and Th17 subpopulations (P4230). J Immunol. 2013;190(1 Supplement).
20. Zhang C, Shao Y, Yang S, Bi X, Li L, Wang H, et al. T-cell tolerance and exhaustion in the clearance of *Echinococcus multilocularis*: Role of inoculum size in a quantitative hepatic experimental model. Sci Rep. 2017 Dec 1;7(1).
21. Zhang C, Lin R, Li Z, Yang S, Bi X, Wang H, et al. Immune Exhaustion of T Cells in Alveolar Echinococcosis Patients and Its Reversal by Blocking Checkpoint Receptor TIGIT in a Murine Model. Hepatology. 2019; hep.30896.
22. Zhou S, Jin X, Li Y, Li W, Chen X, Xu L, et al. Blockade of PD-1 Signaling Enhances Th2 Cell Responses and Aggravates Liver Immunopathology in Mice with *Schistosomiasis japonica*. MacDonald AS, editor. PLoS Negl Trop Dis. 2016; 10(10):e0005094.
23. da Fonseca-Martins AM, Ramos TD, Pratti JES, Firmino-Cruz L, Gomes DCO, Soong L, et al. Immunotherapy using anti-PD-1 and anti-PD-L1 in *Leishmania amazonensis*-infected BALB/c mice reduce parasite load. Sci Rep. 2019; 9(1):1–13.
24. Terrazas LI, Montero D, Terrazas CA, Reyes JL, Rodríguez-Sosa M. Role of the programmed Death-1 pathway in the suppressive activity of alternatively activated macrophages in experimental cysticercosis. Int J Parasitol. 2005 Nov 1;35(13):1349–58.

25. Smith P, Walsh CM, Mangan NE, Fallon RE, Sayers JR, McKenzie ANJ, et al. *Schistosoma mansoni* Worms Induce Anergy of T Cells via Selective Up-Regulation of Programmed Death Ligand 1 on Macrophages . J Immunol. 2004; 173(2):1240–8.
26. Joshi T, Rodriguez S, Perovic V, Cockburn IA, Stäger S. B7-H1 Blockade Increases Survival of Dysfunctional $CD8^+$ T Cells and Confers Protection against *Leishmania donovani* Infections. Mansfield JM, editor. PLoS Pathog. 2009; 5(5):e1000431.
27. Lee J, Ahn E, Kissick HT, Ahmed R. Reinvigorating exhausted T cells by blockade of the PD-1 pathway. For Immunopathol Dis Therap. 2015; 6(1–2):7–18.
28. Rehmann P, Gröne A, Lawrenz A, Pagan O, Gottstein B, Bacciarini LN. *Echinococcus multilocularis* in two lowland gorillas (Gorilla g. gorilla). J Comp Pathol. 2003; 129(1):85–8.
29. Sakaguchi S, Wing K, Onishi Y, Prieto-Martin P, Yamaguchi T. Regulatory T cells: how do they suppress immune responses? Int Immunol. 2009; 21(10):1105–11.
30. Liberal R, Grant CR, Longhi MS, Mieli-Vergani G, Vergani D. Regulatory T cells: Mechanisms of suppression and impairment in autoimmune liver disease. IUBMB Life. 2015; 67(2):88–97.
31. Schmidt A, Oberle N, Krammer PH. Molecular mechanisms of treg-mediated T cell suppression. Front Immunol. 2012; 3:51.
32. Dyck L, Wilk MM, Raverdeau M, Misiak A, Boon L, Mills KHG. Anti-PD-1 inhibits $Foxp3^+$ Treg cell conversion and unleashes intratumoural effector T cells thereby enhancing the efficacy of a cancer vaccine in a mouse model. Cancer Immunol Immunother. 2016; 65(12):1491–8.
33. Isaacsson Velho P, Antonarakis ES. PD-1/PD-L1 pathway inhibitors in advanced prostate cancer. Expert Rev Clin Pharmacol. 2018; 11(5):475–86.
34. Goswami S, Aparicio A, Subudhi SK. Immune Checkpoint Therapies in Prostate Cancer. Cancer J. 2016; 22(2):117–20.
35. DiDomenico J, Lamano JB, Oyon D, Li Y, Veliceasa D, Kaur G, et al. The immune

checkpoint protein PD-L1 induces and maintains regulatory T cells in glioblastoma. Oncoimmunology. 2018; 7(7):e1448329.

36. Chevalier MF, Schneider AK, Cesson V, Dartiguenave F, Lucca I, Jichlinski P, et al. Brief Correspondence Conventional and PD-L1-expressing Regulatory T Cells are Enriched During BCG Therapy and may Limit its Efficacy. Eur. Urol. 2018; 74(5): 540-544.
37. Shen T, Zheng J, Liang H, Xu C, Chen X, Zhang T, et al. Characteristics and PD-1 expression of peripheral $CD4^{+}CD127^{lo}CD25^{hi}FoxP3^{+}$ Treg cells in chronic HCV infected-patients. Virol J. 2011; 8(1):279.
38. Wang J, Cardoso R, Marreros N, Müller N, Lundström-Stadelmann B, Siffert M, et al. $Foxp3^{+}$ T regulatory cells as a potential target for immunotherapy against primary infection with *echinococcus multilocularis* eggs. Infect Immun. 2018;86(10):e00542-18.
39. Tuxun T, Wang JH, Lin RY, Shan JY, Tai QW, Li T, et al. Th17/Treg imbalance in patients with liver cystic echinococcosis. Parasite Immunol. 2012; 34(11):520–7.
40. Behar SM. Antigen-specific CD8(+) T cells and protective immunity to tuberculosis. Adv Exp Med Biol. 2013; 783:141–63.
41. Durgeau A, Virk Y, Corgnac S, Mami-Chouaib F. Recent Advances in Targeting CD8 T-Cell Immunity for More Effective Cancer Immunotherapy. Front Immunol. 2018; 9:14.
42. Helft J, Jacquet A, Joncker NT, Grandjean I, Dorothée G, Kissenpfennig A, et al. Antigen-specific T-T interactions regulate CD4 T-cell expansion. Blood. 2008; 112(4):1249–58.
43. Liu L, Zheng Q, Lee J, Ma Z, Zhu Q, Wang Z. PD-1/PD-L1 expression on CD(4+) T cells and myeloid DCs correlates with the immune pathogenesis of atrial fibrillation. J Cell Mol Med. 2015; 19(6):1223–33.
44. Zelante T, Fric J, Wong AYW, Ricciardi-Castagnoli P. Interleukin-2 Production by Dendritic Cells and its Immuno-Regulatory Functions. Front Immunol. 2012;3:161.
45. Granucci F, Feau S, Angeli V, Trottein F, Ricciardi-Castagnoli P. Early IL-2 Production by Mouse Dendritic Cells Is the Result of Microbial-Induced Priming. J Immunol. 2003;

170(10):5075–81.

46. Krenkel O, Tacke F. Liver macrophages in tissue homeostasis and disease. Nat Rev Immunol. 2017; 17(5):306–21.
47. Ju C, Tacke F. Hepatic macrophages in homeostasis and liver diseases: from pathogenesis to novel therapeutic strategies. Cell Mol Immunol. 2016; 13(3):316–27.
48. Kolios G, Valatas V, Kouroumalis E. Role of Kupffer cells in the pathogenesis of liver disease. World J Gastroenterol. 2006;12(46):7413–20.
49. Sica A, Invernizzi P, Mantovani A. Macrophage Plasticity and Polarization in Liver Homeostasis and Pathology. Hepatol. 2014; 59: 2014-2042.
50. Oka M, Ito Y, Pan W, Tabel H. Polyclonal B-cell-activating factors produced by spleen cells of mice stimulated with a cell homogenate of *Trypanosoma gambiense*. Infect Immun. 1987; 55(12):3162–7.
51. Freire-de-Lima CG, Nunes MP, Corte-Real S, Soares MP, Previato JO, Mendonça-Previato L, et al. Proapoptotic Activity of a *Trypanosoma cruzi* Ceramide-Containing Glycolipid Turned on in Host Macrophages by IFN-γ. J Immunol. 1998;161(9): 4909-16.
52. Su L, Li N, Tang H, Lou Z, Chong X, Zhang C, et al. Kupffer cell-derived TNF-α promotes hepatocytes to produce CXCL1 and mobilize neutrophils in response to necrotic cells. Cell Death Dis. 2018; 9(3):323.
53. Dolina JS, Sung S-SJ, Novobrantseva TI, Nguyen TM, Hahn YS. Lipidoid Nanoparticles Containing PD-L1 siRNA Delivered In Vivo Enter Kupffer Cells and Enhance NK and CD8(+) T Cell-mediated Hepatic Antiviral Immunity. Mol Ther Nucleic Acids. 2013; 2(2):e72.
54. Gong J, Cao D, Chen Y, Li J, Gong J, Zeng Z. Role of programmed death ligand 1 and Kupffer cell in immune regulation after orthotopic liver transplantation in rats. Int Immunopharmacol. 2017;48:8–16.
55. Helk E, Bernin H, Ernst T, Ittrich H, Jacobs T, Heeren J, et al. TNFα-Mediated Liver Destruction by Kupffer Cells and Ly6Chi Monocytes during *Entamoeba histolytica*

Infection. Reed S, editor. PLoS Pathog. 2013; 9(1):e1003096.

56. Hui W, Jiang S, Tang J, Hou H, Chen S, Jia B, et al. An Immediate Innate Immune Response Occurred In the Early Stage of *E. granulosus* Eggs Infection in Sheep: Evidence from Microarray Analysis. PLoS One. 2015; 10(8):e0135096.
57. Tosi MF. Innate immune responses to infection. J Allergy Clin Immunol. 2005;116(2):241–9.
58. Palm NW, Medzhitov R. Not so fast: adaptive suppression of innate immunity. Nat Med. 2007; 13(10):1142–4.
59. Sojka DK, Plougastel-Douglas B, Yang L, Pak-Wittel MA, Artyomov MN, Ivanova Y, et al. Tissue-resident natural killer (NK) cells are cell lineages distinct from thymic and conventional splenic NK cells. Elife. 2014;3:e01659.
60. Peng H, Jiang X, Chen Y, Sojka DK, Wei H, Gao X, et al. Liver-resident NK cells confer adaptive immunity in skin-contact inflammation. J Clin Invest. 2013; 123(4):1444–56.
61. Nair S, Fang M, Sigal LJ. The natural killer cell dysfunction of aged mice is due to the bone marrow stroma and is not restored by IL-15/IL-15Rα treatment. Aging Cell. 2015;14(2):180–90.
62. Ni X, Fu B, Zhang J, Sun R, Tian Z, Wei H. Cytokine-Based Generation of $CD49a^{+}Eomes^{-/+}$ Natural Killer Cell Subsets. Front Immunol. 2018; 9:2126.
63. Bancroft GJ, Kelly JP. Macrophage Activation and Innate Resistance to Infection in SCID Mice. Immunobiology. 1994;191(4–5):424–31.
64. Bancroft GJ. The role of natural killer cells in innate resistance to infection. Curr Opin Immunol. 1993;5(4):503–10.
65. Tripp CS, Wolf SF, Unanue ER. Interleukin 12 and tumor necrosis factor α are costimulators of interferon γ production by natural killer cells in severe combined immunodeficiency mice with listeriosis, and interleukin 10 is a physiologic antagonist. Proc Natl Acad Sci. 1993; 90(8):3725–9.
66. Frassanito MA, Silvestris F, Cafforio P, Silvestris N, Dammacco F. IgG M-components in

active myeloma patients induce a down-regulation of natural killer cell activity. Int J Clin Lab Res. 1997; 27(1):48–54.

67. Sawanobori M, Suzuki K, Nakagawa Y, Inoue Y, Utsuyam M, Hirokaw K. Natural Killer Cell Frequency and Serum Cytokine Levels in Monoclonal Gammopathies: Correlation of Bone Marrow Granular Lymphocytes to Prognosis. Acta Haematol. 1997; 98(3):150–4.
68. Nielsen H, Nielsen HJ, Tvede N, Klarlund K, Mansa B, Moesgaard F, et al. Immune dysfunction in multiple myeloma. Reduced natural killer cell activity and increased levels of soluble interleukin-2 receptors. APMIS. 1991; 99(4):340–6.
69. Tinhofer I, Marschitz I, Henn T, Egle A, Blood RG. Expression of functional interleukin-15 receptor and autocrine production of interleukin-15 as mechanisms of tumor propagation in multiple myeloma. Am Soc Hematol. 2000;15(95): 610-8.
70. Magdalena Dumitru I. Medical Treatment of Cystic Echinococcosis. In: Overview on Echinococcosis. IntechOpen; 2020;88545.

Figure Legends

Fig 1. Parasite load associated with liver inflammation in AE mice with PD-L1 blockade.

(A) Parasite weight was determined by wet weight measurement in *E. multilocularis*-infected mice at end time-point and necropsy. Data represent individual mice from a total of 6 mice in each group, with a statistical power ＞0.8. Comparison between groups was performed using a one-way ANOVA for statistical analysis. **P*<0.05. The levels of TNF-α (B), IL-1β (C), Serum IL-6 (D), IFN-γ (E), IL-33 (F) in the livers from AE mice with/without PD-L1 blockade at end of experiment, corresponding non-infected animals as controls. Data represent individual mice from a total of 6 mice in each group, with a statistical power ＞0.8. Comparison between groups was performed using one-way ANOVA with Bonferroni correction for statistical analysis. **P*<0.05. Control: non-infected wild type mice; AE: *E. multilocularis* infected wild type mice; αPD-L1: animals received anti-PD-L1 MAb application with 200 μg/mouse/injection started 6 weeks post infection and was maintained for 8 weeks (application twice/week); ABZ: Animals received ABZ at 200 mg/kg mouse starting 6 weeks post infection and maintained for another 8 weeks (application 5 days/week).

Fig 2. Effector/regulatory T cell immune responses in the liver from AE mice with PD-L1 blockade and/or ABZ.

Frequency of $Foxp3^-$ cells within $CD4^+$ T cells ($CD4^+$ Teff) in the liver (A), CLTA-4^+ cells within $CD4^+$ Teffs in the liver (B), $Foxp3^-$ cells within $CD8^+$ T cells ($CD8^+$ Tcyt) in the liver (C), CLTA-4^+ cells within $CD8^+$ Tcyts in the liver (D), $Foxp3^+$ cells within $CD4^+$ T cells ($CD4^+$ Treg) in the liver (E), CLTA-4^+ cells within $CD4^+$ Tregs in the liver (F), $Foxp3^+$ cells within $CD8^+$ T cells ($CD8^+$ Treg) in the liver (G), CLTA-4^+ cells within $CD8^+$ Tregs in the liver (H) from AE mice with/without PD-L1 blockade and/or ABZ treatment at end of experiment, corresponding non-infected animals as controls.

Data represent individual mice from a total of 6 mice in each group, with a statistical power ＞0.8. Comparison between groups was performed using one-way ANOVA with Bonferroni correction

for statistical analysis. *P<0.05.

Control: non-infected wild type mice; AE: *E. multilocularis* infected wild type mice

Fig 3. Effector/regulatory T cell immune responses in PECs from AE mice with PD-L1 blockade and/or ABZ.

Frequency of $Foxp3^-$ cells within $CD4^+$ T cells ($CD4^+$ Teff) in the PECs (A), CLTA-4^+ cells within $CD4^+$ Teffs in the PECs (B), $Foxp3^-$ cells within $CD8^+$ T cells ($CD8^+$ Tcyt) in the PECs (C), CLTA-4^+ cells within $CD8^+$ Tcyts in the PECs (D), $Foxp3^+$ cells within $CD4^+$ T cells ($CD4^+$ Treg) in the PECs (E), CLTA-4^+ cells within $CD4^+$ Tregs in the PECs (F), $Foxp3^+$ cells within $CD8^+$ T cells ($CD8^+$ Treg) in the PECs (G), CLTA-4^+ cells within $CD8^+$ Tregs in the PECs (H) from AE mice with/without PD-L1 blockade and/or ABZ treatment at end of experiment, corresponding non-infected animals as controls.

Data represent individual mice from a total of 6 mice in each group, with a statistical power ＞0.8. Comparison between groups was performed using one-way ANOVA with Bonferroni correction for statistical analysis. *P<0.05.

Control: non-infected wild type mice; AE: *E. multilocularis* infected wild type mice; PECs: peritoneal exudate cells.

Fig 4. **DCs and Kupffer cells/Macrophages in AE mice with PD-L1 blockade and/or ABZ.**

Frequency of $CD11c^+CD11b^-$ DCs within $CD45^+$ cells (cDC) in the liver (A), $CD11c^+CD11b^+$ DCs within $CD45^+$ cells (pDC) in the liver (B), $CD11b^+CD11c^+$ $F4/80^+$ cells ($CD11c^+$ Kupffer cells) within $CD45^+$ cells in the liver (C), $11c^+CD11b^-$ DCs within $CD45^+$ cells (cDC) in the PECs (D), $CD11c^+CD11b^+$ DCs within $CD45^+$ cells (pDC) in the PECs (E), $CD11b^+CD11c^+$ $F4/80^+$ cells ($CD11c^+$ Macrophages) within $CD45^+$ cells in PECs (F) from AE mice with/without PD-L1 blockade and/or ABZ treatment at end of experiment, corresponding non-infected animals as controls.

Data represent individual mice from a total of 6 mice in each group, with a statistical power ＞0.8. Comparison between groups was performed using one-way ANOVA for statistical analysis.

*P<0.05.

Control: non-infected wild type mice; AE: *E. multilocularis* infected wild type mice; PECs: peritoneal exudate cells.

Fig 5. **NK/NKT cells in AE mice with PD-L1 blockade and/or ABZ.**

Frequency of $NK1.1^+CD3^+$ cells within $CD45^+$ cells (NKT cell) in the liver (A), $CD69^+$ cells within NKT cells in the liver (B), $NK1.1^+CD3^-$ cells within $CD45^+$ cells (NK cell) in the liver (C), $D69^+$ cells within NK cells in the liver (D), $NK1.1^+CD3^+$ cells within $CD45^+$ cells (NKT cell) in the PECs (E), $CD69^+$ cells within NKT cells in the PECs (F), $NK1.1^+CD3^-$ cells within $CD45^+$ cells (NK cell) in the PECs (G), $D69^+$ cells within NK cells in the PECs (H), from AE mice with/without PD-L1 blockade and/or ABZ treatment at end of experiment, corresponding non-infected animals as controls.

Data represent individual mice from a total of 6 mice in each group, with a statistical power ＞0.8. Comparison between groups was performed using one-way ANOVA for statistical analysis.

*P<0.05.

Control: non-infected wild type mice; AE: *E. multilocularis* infected wild type mice; PECs: peritoneal exudate cells.

Fig 6. Schematic presentation of hypothetical role for immune dynamics due to AE and PD-L1 blockade to modulate the host-parasite relationship to improve the outcome of AE.

E. multilocularis infection and/or metabolites induce the up-regulation of Tregs and T cell exhaustion at the chronic infection stage, as demonstrated previously. PD-L1 blockade was shown to be a promising therapeutic approach to treat murine AE by suppressing Treg cells and their function through IL-10, increasing functional T cells, decreasing NK/ NKT cell frequency and activation, enhancing Kupffer cells and pDCs antigen presentation to T cells, and meanwhile by decreasing excessive inflammatory cytokines in the liver to minimize the “self-injury”. Overall,

this led to an improved immune status that controlled the continuous "tumor-like" progression of the parasitic metacestode.

Supporting Information Legends

S1 Fig. Gating strategy for the assessment of different cell populations in the liver

Gating strategy for the assessment of different cell populations showed by FACS dot plots (Left): A gate was firstly positioned around lymphocytes, and $CD45^+$Viability dye^+ cells within this gate were used for identifying whole living immune cells. Frequency of different cell populations was based on the fluorescence signal of different cell marker staining; As shown in the table (Right), $CD45^+CD3^+$ cells were distinguished as T cells (A), $CD3^+NK1.1^+$ cells as NKT cells (B), $CD3^-NK1.1^+$ cells as NK cells (C), $CD3^+CD4^+CD8^-$ cells as $CD4^+$ T cells (D), $CD3^+CD4^-CD8^+$ cells as $CD8^+$ T cells (E), $CD4^+Foxp3^-$ cells within $CD3^+$ T cells as $CD4^+$ Teff cells (F), $CD4^+Foxp3^+$ cells within $CD3^+$ T cells as $CD4^+$ Tregs (G), $CD8^+Foxp3^-$ cells within $CD3^+$ T cells as $CD4^+$ Tcyt cells (H), $CD8^+Foxp3^+$ cells within $CD3^+$ T cells as $CD8^+$ Tregs (I), $CD45^+CD19^+$ cells as B cells (J), $CD11b^-CD19^+$ cells within B cells as $CD11b^-$ B cells (K), $CD11b^+CD19^+$ cells within B cells as $CD11b^+$ B cells (L), $CD11b^+Ly6G^{high}$ cells as Neutrophils (M), $CD11b^-CD11c^+$ cells as cDCs (N), $CD11b^-CD11c^+$ cells as pDCs (O), $CD11b^+CD11c^+$ cells as pDCs (O), $CD11b^+CD11c^+F4/80^+$ cells as $CD11c^+$Kupffer cells/Macrophages (P), FSC-$A^{++}CD11c^-$ cells as Eosinophils (Q), $CD11c^-Ly6C^+CD11b^+$ cells as Monocytes (R), $CD11b^+CD11c^+$ cells as pDCs (O), $CD11c^-CD11b^+$ $Ly6C^+F4/80^+$ cells as $CD11c^-$Kupffer cells/Macrophages (S).

S2 Fig. Histological analyses from the liver and spleen in AE mice with PD-L1 blockade and/or ABZ.

A. Representative picture of the liver from AE mice with PD-L1 blockade and/or ABZ, respective non-infected animals as control (HE staining, magnification 200x High Power Field (HPF)). Few randomly distributed inflammatory infiltrates and/or accumulation of different precursor cells (EMH) are present in mice from all groups (arrow, unspecific finding). Mild vacuolation of

hepatocytes from groups Control- aPD-L1, Control- aPD-L1+ABZ and Control- ABZ (arrowhead) displays a treatment related increased metabolic rate.

B. Representative picture of the spleen from AE mice with PD-L1 blockade and/or ABZ, respective non-infected animals as control (HE staining, magnification 100x HPF). Strongly increased extramedullary hematopoiesis (EMH, arrow) within the white pulp is visible in all infected groups (first row). Mice from AE and AE- aPD-L1 groups present loss of lymph follicles and PALS, whereas activated follicles are visible in the group AE- aPD-L1+ABZ and AE- ABZ(arrowhead). Mild to moderate EMH and regular follicles and PALS are visible in the spleen of non-infected mice (second row).

S3 Fig. Frequency of $CD45^+$ immune cells

Frequency of $CD45^+$ cells in the liver and PECs from AE mice with/without PD-L1 blockade and/or ABZ treatment at end of experiment, corresponding non-infected animals as negative controls. Data represent individual mice from a total of 6 mice in each group, with a statistical power ＞0.8. Comparison between groups was performed using one-way ANOVA for statistical analysis. **P*<0.05.

Control: non-infected wild type mice; AE: *E. multilocularis* infected wild type mice; PECs: peritoneal exudate cells.

S4 Fig. Effector/regulatory T cell immune responses in the liver from AE mice with PD-L1 blockade

Frequency of $Foxp3^-$ cells within $CD4^+$ T cells ($CD4^+$ Teff), $Foxp3^+$ cells within $CD4^+$ T cells ($CD4^+$ Treg), $Foxp3^-$ cells within $CD8^+$ T cells ($CD8^+$ Tcyt), $Foxp3^+$ cells within $CD8^+$ T cells ($CD8^+$ Treg) in the liver from AE mice with/without PD-L1 blockade at a repeated experiment, corresponding non-infected animals as controls.

Data represent individual mice from a total of 6 mice in each group, with a statistical power ＞0.8. Comparison between groups was performed using one-way ANOVA with Bonferroni correction for statistical analysis. **P*<0.05.

Control: non-infected wild type mice; AE: *E. multilocularis* infected wild type mice

S5 Fig. Frequency of IL-10$^+$ and TNF-α$^+$ in CD45$^+$ cells

Frequency of IL-10$^+$ within CD45$^+$ cells in the liver (A) and PECs (B), TNF-α$^+$ within CD45$^+$ cells in the liver (C) and PECs (D) from AE mice with/without PD-L1 blockade and/or ABZ treatment at end of experiment, corresponding non-infected animals as negative controls. Data represent individual mice from a total of 6 mice in each group, with a statistical power ＞0.8. Comparison between groups was performed using a one-way ANOVA for statistical analysis. **P*<0.05.

Control: non-infected wild type mice; AE: *E. multilocularis* infected wild type mice; PECs: peritoneal exudate cells.

S6 Fig. **DCs and Kupffer cells/Macrophages in AE mice with PD-L1 blockade.**

Frequency of CD11c$^+$CD11b$^-$ DCs within CD45$^+$ cells (cDC), PD-1$^+$CD11c$^+$CD11b$^-$ DCs within CD45$^+$ cells, CD11b$^+$CD11c$^+$ F4/80$^+$ cells (CD11c$^+$ Macrophages) within CD45$^+$ cells, PD-1$^+$CD11b$^+$CD11c$^+$ F4/80$^+$ cells (PD-1$^+$CD11c$^+$ Macrophages), NK1.1$^+$CD3$^-$ cells within CD45$^+$ cells (NK cells) in the liver from AE mice with/without PD-L1 blockade at a repeated experiment, corresponding non-infected animals as controls.

Data represent individual mice from a total of 6 mice in each group, with a statistical power ＞0.8. Comparison between groups was performed using one-way ANOVA for statistical analysis. **P*<0.05.

Control: non-infected wild type mice; AE: *E. multilocularis* infected wild type mice.

S7 Fig. CD49a$^+$ and CD49b$^+$ cell levels in ILC-1 and NK cells in the liver from AE mice with PD-L1 blockade and/or ABZ

Representative images of CD49a$^+$ and CD49b$^+$ cells within ILC-1 and NK cells in the liver (A), mean fluorescence intensity (MFI) of CD49a$^+$ and CD49b$^+$ cells within ILC-1 and NK cells in the

liver (B) from AE mice with/without PD-L1 blockade at end of experiment, corresponding non-infected animals as controls.

Data represent individual mice from a total of 6 mice in each group, with a statistical power ＞0.8. Comparison between groups was performed using one-way ANOVA for statistical analysis. *P<0.05.

Control: non-infected wild type mice; AE: *E. multilocularis* infected wild type mice; PECs: peritoneal exudate cells.

Table. 1 Antibodies used for FACS staining

Fluorescence	Cell marker	Clone	Company	Catalog no.
Alexa Fluor 700	NK1.1	PK136	BioLegend	108730
PE-cy5	NK1.1	PK136	BioLegend	108716
PE-efluor-610	Eomes	Dan11mag	eBioscience	61-4875-82
APC	Roryt	AFKJS-9	eBioscience	17-6988-80
APC-efluor780	PD-1	J43	eBioscience	47-9985-82
PE-cy7	CD49b	DX5	BioLegend	108922
PE-cy7	CD4	GK1.5	eBioscience	25-0041-81
APC	CD4	RM4-4	BioLegend	116014
BV570	CD8	53-6.7	BioLegend	301038
Alexa Fluor 700	CD11b	M1/70	BioLegend	101222
BV421	CD49a	Ha31/8	BD Biosciences	740046
PE	CD19	SJ25C1	eBioscience	12-0198-41
PE-Dazzle 594	CD19	6D5	BioLegend	115554
BUV395	CD45	30-F11(Ruo)	BD Biosciences	564279
Percp cy.5.5	FoxP3	FJK-16s	eBioscience	45-5773-80
PE	FoxP3	FJK-16s	eBioscience	12-5773-80
PE-Dazzle 594	CD152	UC10-4B9	BioLegend	106318
APC	IL-10	JES5-16E3	BioLegend	505010
PE	IL-10	JES3-9D7	eBioscience	12-7108-41
FITC	CD69	H1.2F3	BioLegend	104506
PE	Ly6G	RB6-8C5	eBioscience	12-8931-81
PE-cy7	Ly6G	RB6-8C5	eBioscience	25-5931-81
APC	F4/80	BM8	eBioscience	17-4801-82
eFluor450	CD11c	N418	eBioscience	48-0114-82
FITC	TNFα	MP6-XT22	BioLegend	506304
eFluor506	VIABILITY DYE	-	eBioscience	65-0866-18
-	CD16/CD32	2.4 G2	BioLegend	101302

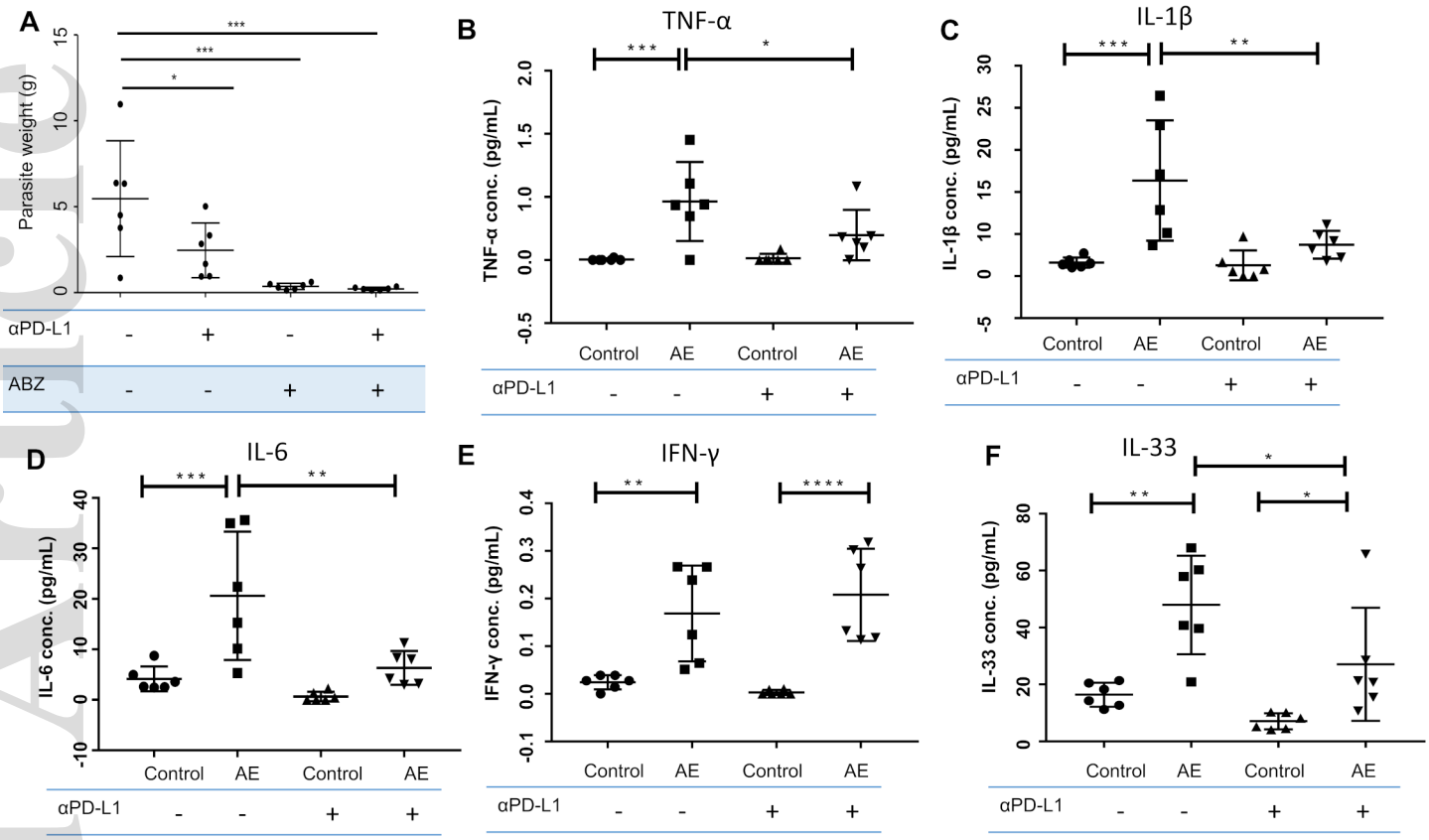

pim_12834_f1.tif

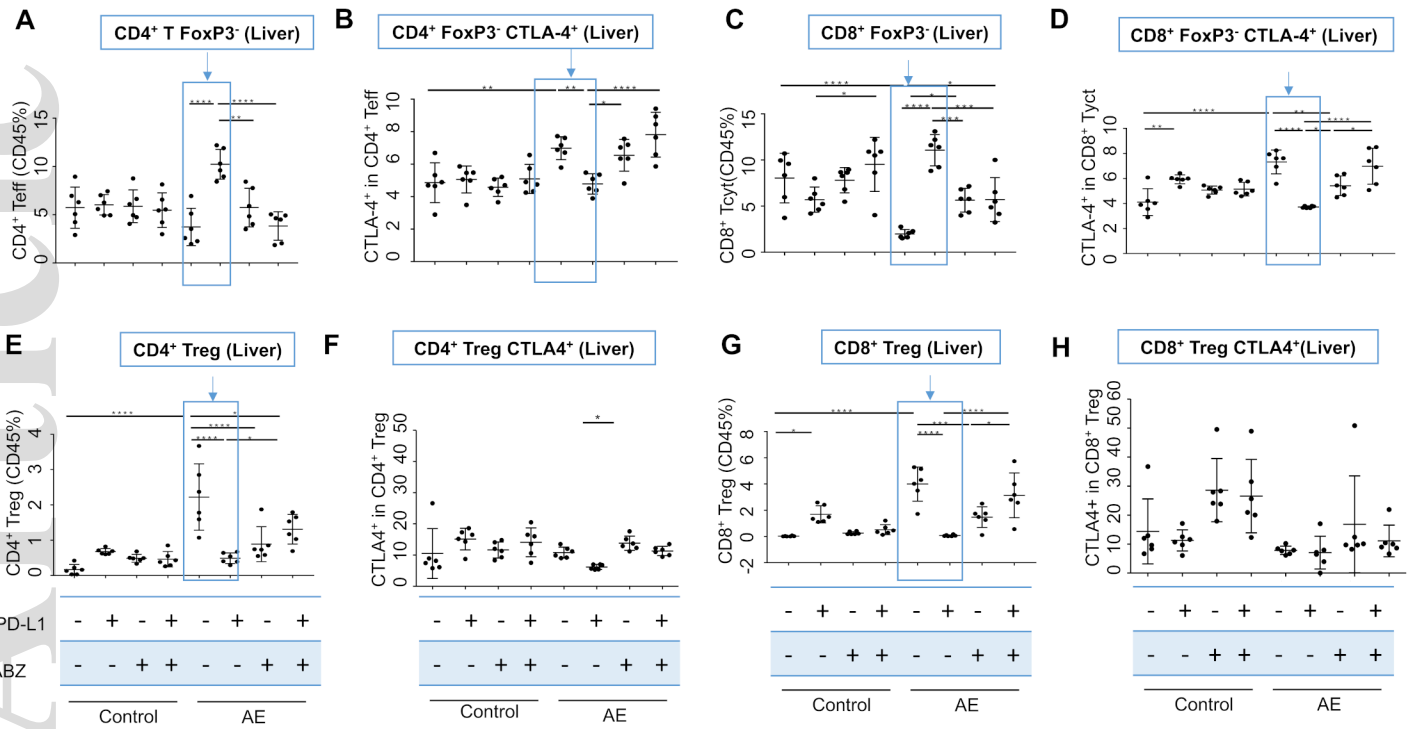

pim_12834_f2.tif

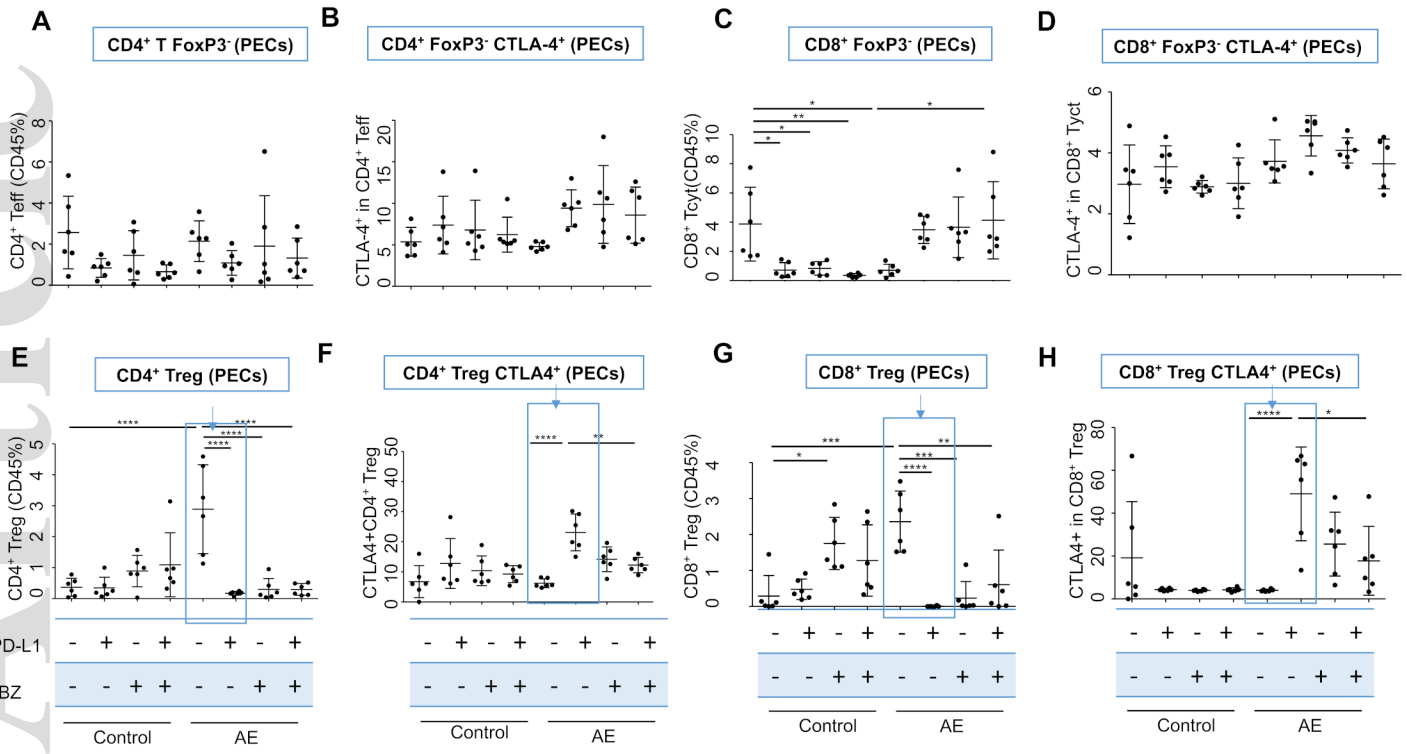

pim_12834_f3.tif

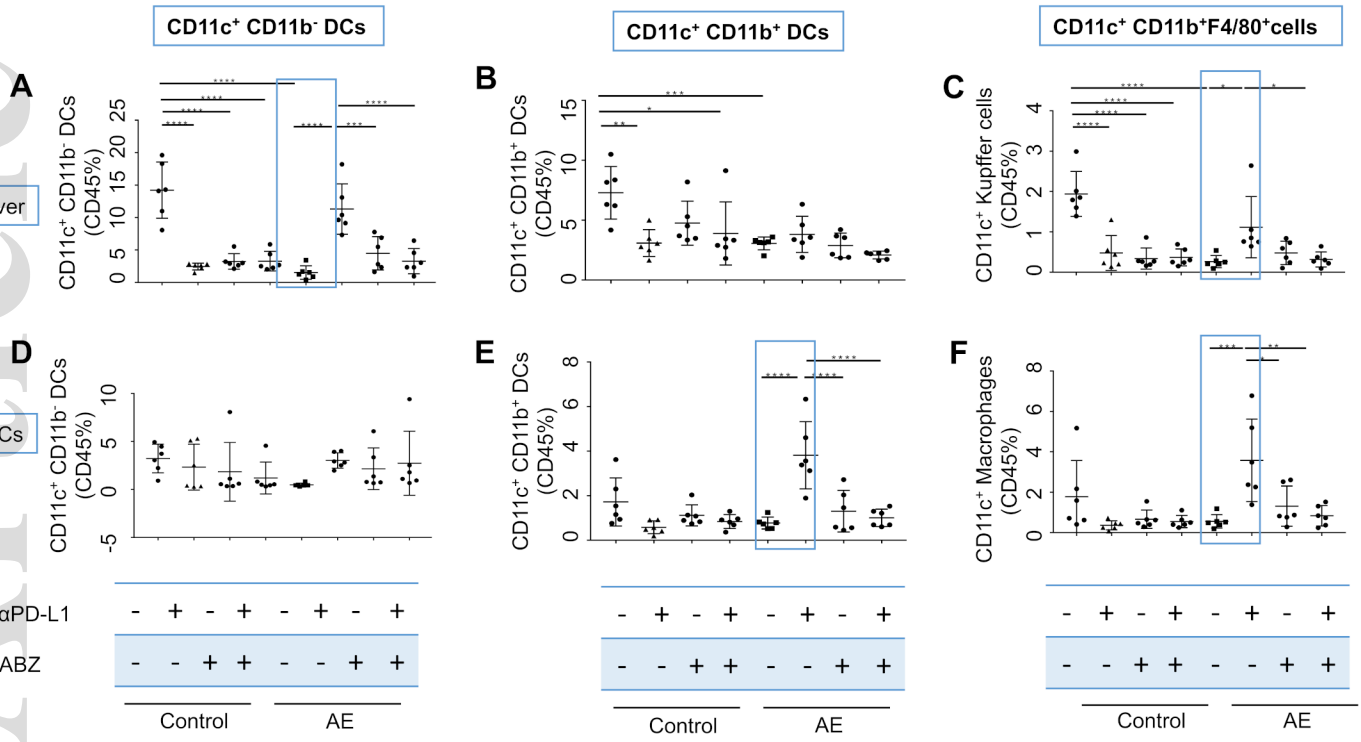

pim_12834_f4.tif

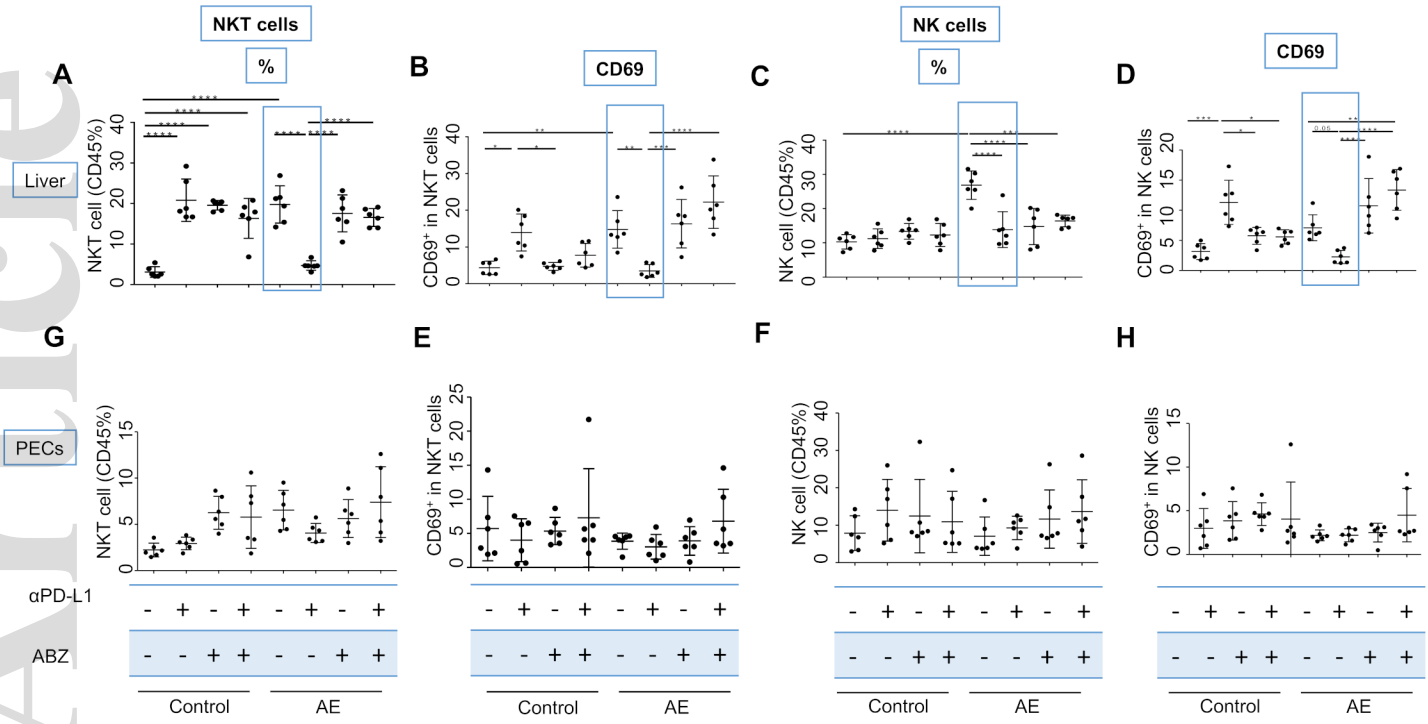

pim_12834_f5.tif

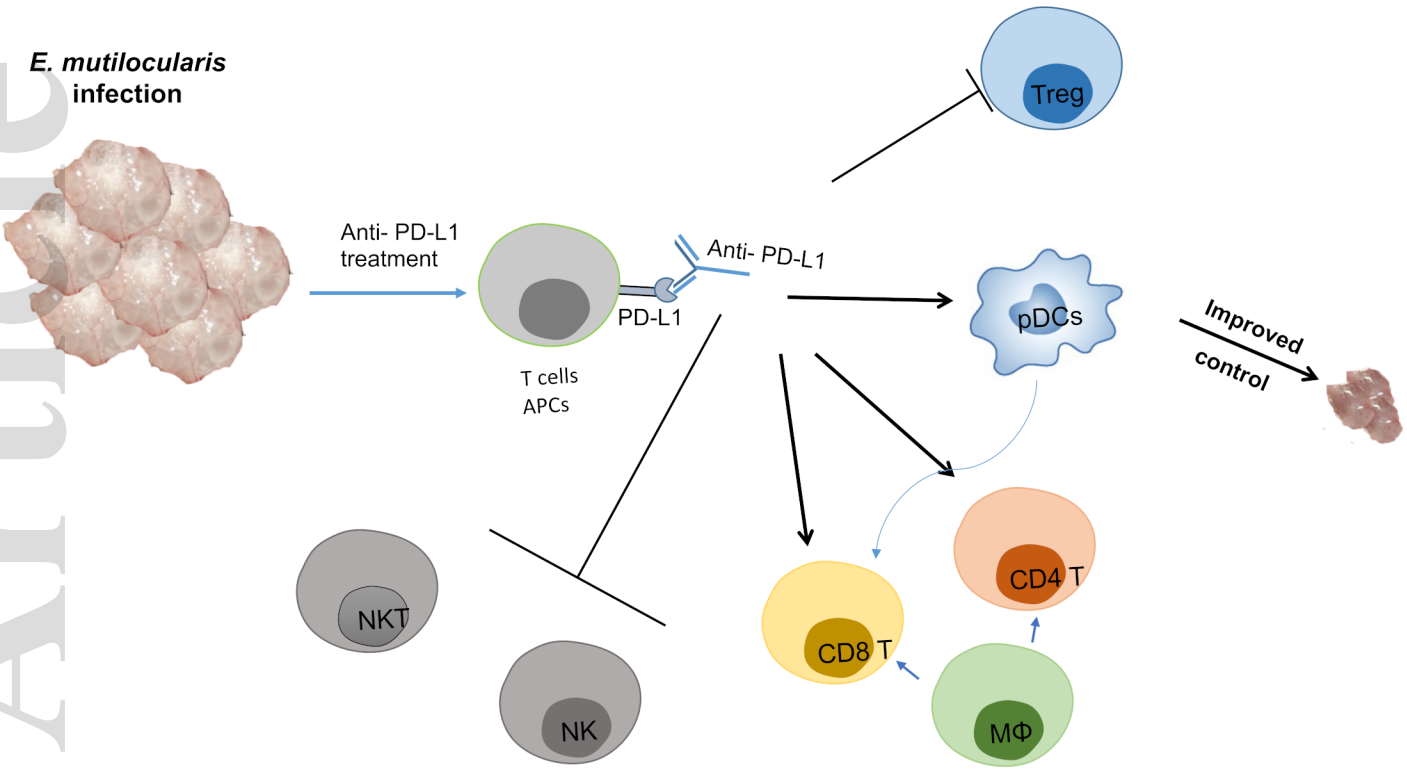

pim_12834_f6.tif